Orthorhombic symmetry components in the ligand field of a macrocyclic tetraimine copper(II) complex

A. Ceulemans[a,*], R. Debuyst[b], F. Dejehet[b], G. S. D. King[c], M. Vanhecke[a,c] and L. G. Vanquickenborne[a]

[a]*Quantum Chemistry Laboratory, University of Leuven, Celestijnenlaan 200F&C, B-3001 Leuven (Belgium)*
[b]*Laboratoire de Chimie Inorganique et Nucléaire, Université de Louvain, Chemin du Cyclotron 2, B-1348 Louvain-la-Neuve (Belgium)*
[c]*Crystallography Laboratory, University of Leuven, Celestijnenlaan 200F&C, B-3001 Leuven (Belgium)*

(Received June 13, 1991; revised October 14, 1991)

Abstract

The single-crystal EPR spectrum of the tetraimine macrocyclic Cu(II) complex $[Cu(C_{10}H_{20}N_8)Cl]Cl$ has been measured, both in the lattice of the pure compound and of the isomorphous Ni(II) compound. The crystal structure of the Cu(II) complex has also been determined. The space group is $P\bar{1}$, with $a=7.574(1)$, $b=9.548(1)$, $c=11.469(1)$ Å, $\alpha=96.32(1)$, $\beta=107.19(1)$, $\gamma=99.67(2)°$ and $Z=2$. The ^{63}Cu-doped $[Ni(C_{10}H_{20}N_8)Cl]$ compound has an anisotropic EPR spectrum with $g_1=2.178, g_2=2.066, g_3=2.048$ and $A_1=175, A_2=48, A_3=22$ G. Superhyperfine interactions with the nitrogen ligators were also observed. The g values for the pure compound are almost the same as for the diluted compound. The axial g_1 and A_1 vectors are nearly collinear, whereas the equatorial g_2, g_3 and A_2, A_3 components are at about 45° from each other, the g eigenvectors lying approximately along the bond directions. These features of the spectrum indicate the presence of orthorhombic symmetry components in the ligand field of the macrocycle. These components have been studied with the aid of a detailed ligand field model, taking into account the anisotropic π-bonding of unsaturated chelates.

1. Introduction

The macrocyclic tetraimine ligand $C_{10}H_{20}N_8$ (**1**) forms square planar complexes with the divalent ions of first-row transition-metals Fe, Co, Ni and Cu [1]. These complexes may bind additional ligands at their free coordination sites to yield five-coordinate square pyramidal or six-coordinate octahedral structures.

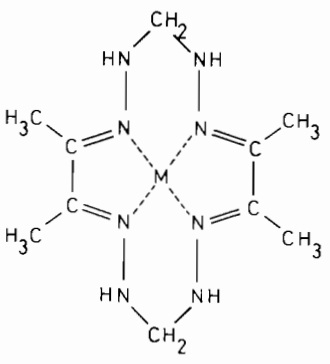

1

The sequence of $M(C_{10}H_{20}N_8)Cl_2$ compounds forms an interesting basis for a comparative study of the ligand field characteristics of a tetraimine macrocycle. The four nitrogen atoms typically exert a very strong equatorial field at their centre of gravity. This field, which has only approximate fourfold symmetry, stabilizes low spin states of the central metal ion. In order to account for the observed anisotropy of the molecular g and A tensors in the Co^{2+} and Cu^{2+} complexes of this macrocycle, ligand field components of orthorhombic symmetry must also be present. These components require special attention since they are intimately related to the nature of the macrocyclic coordination. In principle, two different orthorhombic perturbations must be envisaged: firstly, the geometric distortions of the macrocyclic cavity, and secondly, the specific electronic effects of double bonding in the α-diimine strands of the ligand ring. These electronic effects have been shown to control the spatial orientation of the molecular g tensor in the low-spin d^7 $Co(C_{10}H_{20}N_8)Cl_2$ complex [2]. In the present study we extend the measurement of g-factor anisotropy to the analogous d^9 $Cu(C_{10}H_{20}N_8)Cl_2$ complex. Copper as a central metal ion is expected to be a more sensitive EPR probe than cobalt for the geometrical distortions of axial symmetry.

*Author to whom correspondence should be addressed.

0020-1693/92/$5.00

2. Experimental

2.1. Synthesis

Goedken and co-workers [1] have described a convenient method for the synthesis of $Ni(C_{10}H_{20}N_8)Cl_2$. This method is equally applicable to the analogous $Cu(C_{10}H_{20}N_8)Cl_2$ complex. In order to obtain crystals, the reaction mixture was left standing overnight, after which the precipitate was filtered off. Small crystals could be grown from the remaining solution in a few days. For the EPR measurements, single crystals of the diamagnetic $Ni(C_{10}H_{20}N_8)Cl_2$ complex, doped with Cu(II) were prepared from a mixture of $CuCl_2 \cdot 6H_2O$ and $NiCl_2 \cdot 6H_2O$ in a 5:95 molar ratio. Atomic absorption spectrometric analysis showed that the Cu:Ni ratio in the doped crystals was the same as the initial ratio of the reagents. In one experiment we used isotopically pure $^{63}CuCl_2$ as a dopant, in order to improve the resolution of the EPR spectra. The $Cu(C_{10}H_{20}N_8)Cl_2$ complex was characterized by UV–vis and IR spectroscopy. In aqueous solution the UV–vis spectra of this chromophore are virtually identical to the reported spectra for the dissolved $[Cu(C_{10}H_{20}N_8)Cl(H_2O)](ClO_4)$ complex [1]. IR spectrometry of the solid material in nujol mulls shows a close similarity between the vibrational structures of $Cu(C_{10}H_{20}N_8)Cl_2$ and of $Ni(C_{10}H_{20}N_8)Cl_2$.

2.2. Crystal structure determination

All diffraction measurements were made on an irregularly shaped crystal of about 0.2 mm diameter using a Syntex $P2_1$ diffractometer with graphite-monochromatized radiation ($\lambda = 1.54183$ Å). The crystal density was determined by flotation in a $CCl_4/CHBr_3$ mixture. Cell parameters were determined by least-squares refinement of the 2θ values of 24 reflections. Crystal data: $C_{10}H_{20}N_8 \cdot CuCl_2$, $M = 386.77$, $a = 7.574(1)$, $b = 9.548(1)$, $c = 11.469(1)$ Å, $\alpha = 96.32(1)$, $\beta = 107.19(1)$, $\gamma = 99.67(2)°$, $V = 769.8$ Å^3. Space group $P\bar{1}$, $Z = 2$, $D_m = 1.68(1)$, $D_c = 1.669$ g cm^{-3}. Intensities of all 3708 reflections to sin $\theta/\lambda = 0.525$ were measured using the $\theta/2\theta$ scan method. After application of an empirical absorption correction and taking account of Lorentz and polarization factors, symmetry-equivalent reflections were averaged to give 1859 independent intensities of which 1787 had an intensity exceeding twice the standard deviation and were considered as observed.

The positions of the copper and chlorine atoms were found by Patterson methods and those of the nitrogen and carbon atoms by Fourier methods. The coordinates and isotropic displacement parameters of these atoms were refined by full matrix least-squares methods. A difference electron density map did not give a clear indication of the positions of the hydrogen atoms so these were placed at calculated positions assuming C–H and N–H distances of 1.05 and 0.95 Å, respectively. The hydrogen atoms were assigned isotropic displacement parameters 20% greater than those of the atoms to which they are bonded. Full-matrix least-squares refinement of positional and anisotropic displacement parameters of the non-hydrogen atoms led to a final R value of 0.045. All crystallographic calculations were carried out with the XTAL 2.6 system [3].

2.3. EPR spectroscopy

Single crystals of $[Cu(C_{10}H_{20}N_8)Cl]Cl$ and of $[Ni(C_{10}H_{20}N_8)Cl]Cl$ doped with $^{63}Cu(II)$ were glued to a 27 mm^3 perspex cube, mounted on a perspex rod that was itself inserted in a goniometer. This setting allows the rotation of the samples about three perpendicular axes. For each rotation, EPR spectra were recorded at 10° intervals, from 0 to 180°. All single crystal measurements were performed at room temperature; some spectra of powdered material were also registered at 77 K and room temperature.

A Bruker X-band ER 200tt spectrometer was used. The magnetic field was measured with a Bruker B-NM 12 NMR oscillator; the measurement of the klystron frequency was achieved with a 12.5 MHz 5216 A Hewlett-Packard frequency counter and a 1/1000 5260 A Hewlett-Packard frequency divider. The crystallographic axes were positioned by Weissenberg techniques. The crystals showed a well-developed face, containing two crystallographic axes; this feature facilitated the orientation of the samples.

3. Results

3.1. Description of the crystal structure

The final atomic coordinates and equivalent isotropic displacement parameters for the $Cu(C_{10}H_{20}N_8)Cl_2$ complex are given in Table 1 and selected bond lengths and angles in Table 2. An overview of the molecular geometry is represented in Fig. 1.

The Cu(II) ion is surrounded by five ligator atoms in a distorted square pyramidal arrangement. The approximate C_{2v} symmetry of the complex will be discussed in Section 4. The two CH_2 groups point upwards in a boat-like conformation. The Cu(II) ion is 0.46 Å above the plane of the four nitrogen ligands. Apparently this raising of the central metal induces a concomitant bowing of the macrocycle.

Similar structural characteristics have been observed in various other tetraimine complexes of Cu(II). In the $[Cu(TIM)Cl]PF_6$ complex [4] (2) the Cu(II) ion is displaced 0.34 Å from the basal plane and the Cu–Cl bond length is 2.404 Å. In this case boat and chair conformations coexist in the crystal. The uninegative cyclops ligand (3), a tetraimine macrocycle with a

TABLE 1. Atomic coordinates and isotropic displacement parameters for the non-hydrogen atoms in $[Cu(C_{10}H_{20}N_8)]Cl_2$. Standard deviations for the last digit are given in parentheses

	x/a	y/b	z/c	$U\times100$ (Å^2)
Cu	0.6187(1)	0.34335(1)	0.25366(1)	2.42(4)
Cl1	0.2877(2)	0.3135(1)	0.1449(1)	3.02(6)
Cl2	0.0472(2)	0.9254(1)	0.3360(1)	4.14(7)
N1	0.7255(6)	0.4003(4)	0.1230(4)	2.4(2)
N2	0.7557(6)	0.5421(4)	0.1056(4)	3.1(2)
C3	0.6473(8)	0.6289(6)	0.1588(5)	3.4(3)
N4	0.7107(6)	0.6613(4)	0.2920(4)	3.1(2)
N5	0.6949(6)	0.5420(4)	0.3481(4)	2.4(2)
C6	0.7491(7)	0.5527(5)	0.4662(5)	2.7(3)
C7	0.7259(7)	0.4120(6)	0.5101(5)	2.6(2)
C8	0.8292(9)	0.6916(6)	0.5539(5)	4.2(3)
C9	0.7748(9)	0.4008(6)	0.6444(5)	4.1(3)
N10	0.6580(6)	0.3004(4)	0.4227(4)	2.4(2)
N11	0.6340(6)	0.1626(5)	0.4478(4)	3.1(2)
C12	0.5464(8)	0.0515(5)	0.3381(5)	3.1(2)
N13	0.6493(6)	0.0365(4)	0.2500(4)	3.1(2)
N14	0.6678(6)	0.1578(4)	0.1929(4)	2.5(2)
C15	0.7392(7)	0.1563(5)	0.1037(5)	2.7(2)
C16	0.7612(7)	0.2973(6)	0.0576(5)	2.8(2)
C17	0.7930(9)	0.0309(6)	0.0484(5)	4.2(3)
C18	0.8221(8)	0.3062(6)	−0.0549(5)	3.5(3)

difluoro–borate linkage, forms square pyramidal Cu(II) complexes with various adducts [5, 6]. In the cyanato complex, Cu(cyclops)(NCO), the raising of the central metal above the N_4 plane is 0.58 Å, which is the largest axial displacement of Cu(II) yet reported [5].

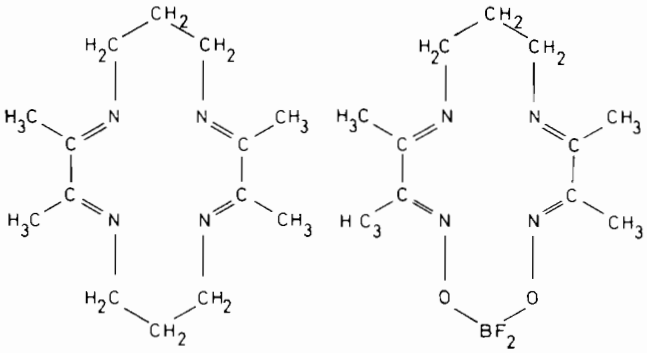

2 TIM

3 CYCLOPS

Comparison of the present Cu(II) complex with the analogous $Ni(C_{10}H_{20}N_8)Cl_2$ complex [2] is instructive. These two complexes are nearly isostructural, as is borne out by the similarity of their IR spectra. The main difference is that the Ni(II) is only 0.28 Å above the basal plane, compared with the 0.46 Å displacement of Cu(II). The dimensions of the pyramid with Cl1 at the apex and N1, N5, N10 and N14 forming the base are very similar in the two compounds with Cl–N distances of 3.37, 3.48, 3.60 and 3.39 Å in the copper compound and 3.31, 3.46, 3.53 and 3.33 Å in the nickel one. The lesser degree of planarity in the copper

TABLE 2. Selected bond lengths (Å) and angles (°) for $[Cu(C_{10}H_{20}N_8)]Cl_2$

Cu–Cl1	2.399(1)	N1–Cu–N5	92.8(2)
		N5–Cu–N10	80.3(2)
Cu–N1	1.986(5)	N10–Cu–N14	93.0(2)
Cu–N5	1.979(4)	N14–Cu–N1	80.1(2)
Cu–N10	1.972(4)		
Cu–N14	1.966(4)	Cu–N1–N2	120.7(4)
		Cu–N5–N4	122.3(3)
Cl1–N1	3.370(5)	Cu–N10–N11	122.9(3)
Cl1–N5	3.475(4)	Cu–N14–N13	123.4(3)
Cl1–N10	3.600(4)	Cu–N1–C16	115.5(4)
Cl1–N14	3.389(5)	Cu–N5–C6	115.7(4)
		Cu–N10–C7	114.9(4)
N1–C16	1.284(7)	Cu–N14–C15	116.3(4)
N5–C6	1.281(7)		
N10–C7	1.297(6)	Cl1–Cu–N1	100.0(1)
N14–C15	1.291(8)	Cl1–Cu–N5	104.7(1)
		Cl1–Cu–N10	110.5(1)
N1–N2	1.381(6)	Cl1–Cu–N14	101.4(1)
N4–N5	1.374(6)		
N10–N11	1.372(6)		
N13–N14	1.398(6)		
C3–N2	1.465(8)		
C3–N4	1.440(7)		
C12–N11	1.458(6)		
C12–N13	1.456(9)		
C6–C7	1.487(8)		
C6–C8	1.488(7)		
C7–C9	1.494(8)		
C15–C16	1.501(8)		
C15–C17	1.467(9)		
C16–C18	1.499(9)		

compound involves longer metal–ligator bonds (1.98 Å compared with 1.89 Å) and shorter metal chloride bonds (2.40 and 2.57 Å, respectively) than in the nickel compound. This suggests that Ni^{2+} has a stronger tendency to form square planar complexes than does Cu^{2+}. As pointed out by Anderson and Marshall [5], the severe out-of-plane displacement of the Cu(II) ion could be related to the population by one electron of the d_{xy} orbital, which is antibonding in the equatorial plane.

The unit cell contains two equivalent molecules related by an inversion centre. The $Cu(C_{10}H_{20}N_8)Cl_2$ structure is clearly isomorphous with the previously published [2] $Ni(C_{10}H_{20}N_8)Cl_2$ structure, as can be gathered from a comparison of the cell parameters. This is confirmed by the EPR data for the pure $Cu(C_{10}H_{20}N_8)Cl_2$ and diluted $Ni_{0.95}Cu_{0.05}(C_{10}H_{20}N_8)Cl_2$ crystals.

3.2. EPR spectroscopy

3.2.1. Doped compound $[Ni_{0.95}{}^{63}Cu_{0.05}(C_{10}H_{20}N_8)Cl]Cl$

The use of pure isotopic ^{63}Cu for doping should improve the resolution of the EPR spectra, given the

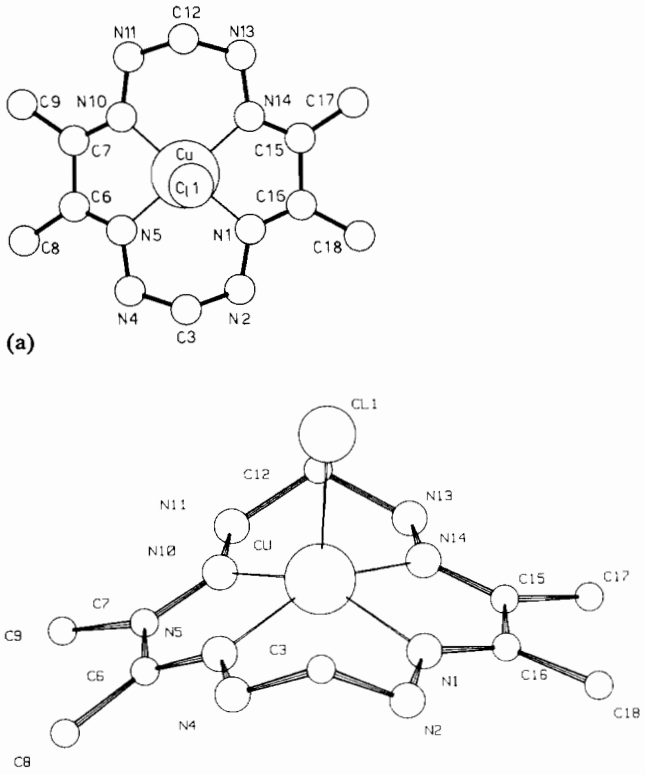

Fig. 1. Drawings of the $Cu(C_{10}H_{20}N_8)Cl^+$ cation. The symmetry is nearly C_{2v}. Bond distances and angles are given in Table 2.

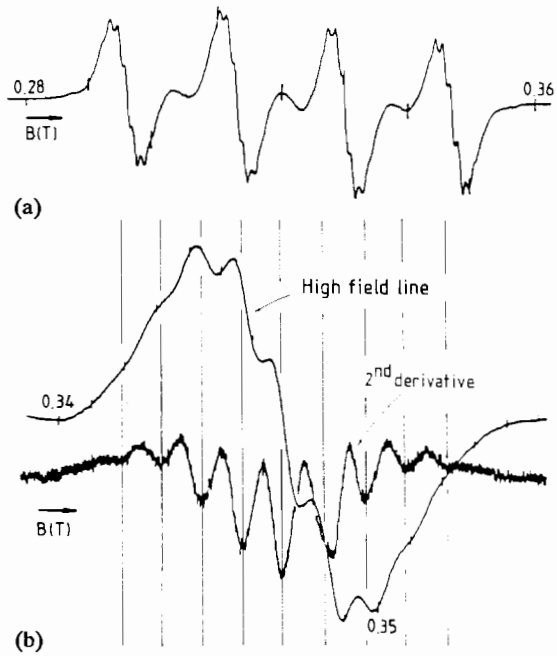

Fig. 2. Typical EPR spectrum of ^{63}Cu-doped $[Ni(C_{10}H_{20}N_8)Cl]Cl$ showing the four hyperfine components (a). First and second derivative spectra showing the nine superhyperfine components superimposed on the high field hyperfine line (b). Intensities are approximately proportional to 1,4,10,16,19,16,10,4,1 (magnetic field in Tesla).

TABLE 3. Principal values and axes[a] for the g, copper hyperfine and nitrogen superhyperfine tensors for the doped compound

		a	b'	c'
g	$g_1=2.178\pm0.002$	0.92	0.07	0.39
	$g_2=2.066\pm0.006$	0.36	0.26	−0.89
	$g_3=2.048\pm0.006$	−0.16	0.96	0.22
Hyperfine Cu	$A_1=175\pm1$ G	0.91	0.07	0.41
	$A_2=48\pm10$ G	0.40	−0.42	−0.81
	$A_3=22\pm10$ G	0.11	0.90	−0.41
Superhyperfine N	$A_1=13\pm1$ G	0.91	0.24	0.35
	$A_2=16\pm1$ G	0.42	−0.35	−0.84
	$A_3=14\pm1$ G	−0.08	0.90	−0.42

[a]The experimental error on the measured principal directions is of the order of 5°. The three axes a, b', c' form an orthogonal system, with b' perpendicular to a in the (a, b) plane of the host lattice.

closeness of the nuclear magnetic moments of the two constituent isotopes of natural copper. Owing to the presence in the unit cell of only two molecules related by an inversion centre, the EPR spectrum is that of a single magnetic species yielding four hyperfine lines ($S=1/2$, $I_{Cu}=3/2$) split into 9 superhyperfine components reflecting the interaction of the magnetic electron with four equivalent nitrogen atoms ($I_N=1$). A typical spectrum is shown in Fig. 2. The anisotropy of the hyperfine interaction with the ^{63}Cu nucleus causes the four hyperfine components to coalesce into a single broad line in many measurement directions. It follows that the estimation of the centre of the spectrum (g value) as well as of the distance between the hyperfine components was often very difficult. The superhyperfine coupling value was estimated from the extreme components on the high field hyperfine line, in second derivative spectra. As can be seen from Fig. 2, the linewidths are about 40 and 8 G for copper and nitrogen interactions, respectively. The procedure followed for the estimation of the g^2 and g^2A^2 tensor elements and their diagonalization is described in ref. 7. This first order analysis of the data gives the eigenvalues and eigenvectors in Table 3.

A drawing of the g and A_{Cu} eigenvectors with respect to the molecular bonds is shown in Fig. 3(a). The principal axes corresponding to the largest g and A_{Cu} are nearly collinear and perpendicular to the ligator plane. In the equatorial plane there is a remarkable non-coincidence of the g and A_{Cu} directions. The g_2 and g_3 axes lie approximately along the bond directions, while the A_{Cu} axes are close to the molecular x and y axes. Hence the equatorial components of the g and A_{Cu} tensors are at about 45° from each other. The superhyperfine eigenvectors, which are not represented, lie close to those of the copper hyperfine tensor.

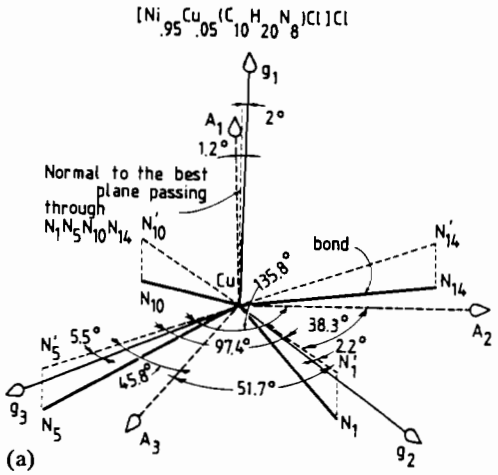

(a)

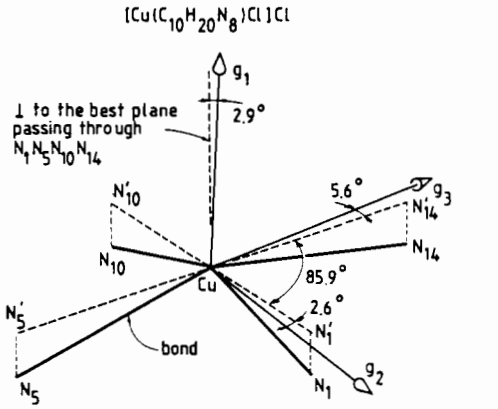

CuN_i' = projection of CuN_i on the plane containing Cu parallel to the best plane passing through the tetra-imine nitrogens $N_1N_5N_{10}N_{14}$

(b)

Fig. 3. Position of the eigenvectors as compared to the metal bonds in $^{63}Cu(II)$-doped $[Ni(C_{10}H_{20}N_8)Cl]Cl$ (a) and in pure $[Cu(C_{10}H_{20}N_8)Cl]Cl$ (b). The N' symbols denote the projection of the N ligators on the plane containing Cu parallel to the best plane passing through the N1, N5, N10, N14 atoms.

Powder spectra have been measured at room temperature and 77 K (which showed no substantial improvement), from which $g_{\parallel}$, $g_{\perp}$ and $A_{\parallel}^{Cu}$ values could be estimated that are in satisfactory agreement with the single crystal values.

3.2.2. Pure compound $[Cu(C_{10}H_{20}N_8)Cl]Cl$

As usual in magnetically non-diluted compounds, only a single line is observed. The hyperfine components are lost because of exchange interaction between the paramagnetic species. The line width fluctuates from ~15 to ~30 G. Treatment of the rotational data as described in ref. 7 yields the principal values and the orientation of the g^2 tensor: $g_1=2.183$, $g_2=2.066$, $g_3=2.047$, i.e. the same values as for the diluted compound, given the order of the experimental errors (0.005). Because of the inversion centre linking the two molecules in the unit cell, the crystal g values coincide with the molecular g values. The positions of the g eigenvectors compared with the chemical bonds are given in Fig. 3(b). A powder spectrum measured at room temperature shows the familiar picture of an axial paramagnetic species with $g_{\parallel}=2.183$ and $g_{\perp}\sim2.047$.

4. Ligand field model

4.1. Coordinate frame

The choice of a convenient coordinate frame is an important first step in the construction of a suitable ligand field model. The axis of greatest inertia of the system of four ligator atoms N1, N5, N10 and N14 is defined as the molecular z axis. The coordinate origin is placed on the central metal ion, the xy plane thus being parallel to the best plane through the four nitrogen ligators. The y axis is oriented along the bisector of the α-diimine bite angles (**4**). The orientation of this system is in line with the conventions adopted in ref. 2.

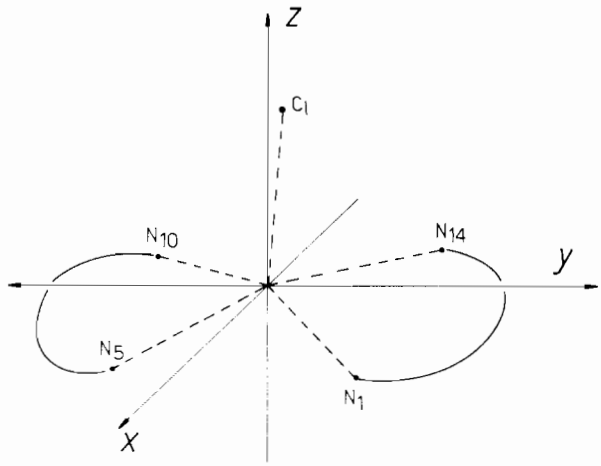

4

The polar coordinates R,θ and φ of the five ligator atoms in the molecular xyz frame are given in Table 4. These coordinates refer to the coordination geometry of the Cu^{2+} ion in the undiluted compound. The close

TABLE 4. Polar coordinates of the five ligators in the CuN_4Cl^+ unit

Ligator[a]	R (Å)	θ (°)	φ (°)
N1	1.986	105.2	48.4
N5	1.979	103.1	−48.2
N10	1.972	105.3	−131.6
N14	1.966	103.1	131.6
Cl	2.399	5.3	60.3

[a]Ligator atoms are numbered as indicated in Fig. 1.

similarity of the molecular g tensors in pure and doped crystals suggests that the same coordination geometry also applies to the Cu^{2+} ion in the diluted samples.

The distribution of the φ angles for the four nitrogens has almost exact C_{2v} symmetry. The corresponding holohedrized symmetry group is D_{2h}, with its mirror planes along the three Cartesian coordinates planes. However the distribution of the R and θ values is less symmetric. The average bond length along the N1–Cu–N10 axis is somewhat larger (0.006 Å) than the bond length along the N5–Cu–N14 axis. The longer axis is more bent too, as indicated by the larger θ values for N1 and N10. Finally it should be noted that the apical Cl ligand is slightly displaced from the z axis in the direction of the Cu–N1 bond.

4.2. Matrix elements

The macrocyclic ligand contains two unsaturated α-diimine strands, which give rise to specific anisotropic π-bonding interactions with the d-orbitals. The ligand field matrix elements of these strands can most easily be obtained when starting from a reference position, as depicted in Fig. 4.

The ligand field perturbation matrix $\mathscr{H}_{NN}$ for one single strand along the positive y axis of this reference position [8] is specified in eqn. (1).

$$\mathscr{H}_{NN}= \begin{array}{c} \begin{matrix} \quad d_{z^2} & \quad d_{yz} & \quad d_{xz} & \quad d_{xy} & \quad d_{x^2-y^2} \end{matrix} \\ \begin{bmatrix} \frac{1}{2}e_\sigma^N & 0 & 0 & 0 & \frac{\sqrt{3}}{2}\cos\delta e_\sigma^N \\ 0 & 2\cos^2\frac{\delta}{2}e_\psi^N & 0 & 0 & 0 \\ 0 & 0 & 2\sin^2\frac{\delta}{2}e_x^N & 0 & 0 \\ 0 & 0 & 0 & 2\cos^2\delta e_{\pi\|}^N + \frac{3}{2}\sin^2\delta e_\sigma^N & 0 \\ \frac{\sqrt{3}}{2}\cos\delta e_\sigma^N & 0 & 0 & 0 & 2\sin^2\delta e_{\pi\|}^N + \frac{3}{2}\cos^2\delta e_\sigma^N \end{bmatrix} \end{array} \tag{1}$$

$$\mathbb{F}(\mathscr{R}_\alpha^x)= \begin{bmatrix} \frac{1+3\cos 2\alpha}{4} & \frac{\sqrt{3}}{2}\sin 2\alpha & 0 & 0 & \frac{\sqrt{3}}{4}(\cos 2\alpha-1) \\ -\frac{\sqrt{3}}{2}\sin 2\alpha & \cos 2\alpha & 0 & 0 & -\frac{1}{2}\sin 2\alpha \\ 0 & 0 & \cos\alpha & \sin\alpha & 0 \\ 0 & 0 & -\sin\alpha & \cos\alpha & 0 \\ \frac{\sqrt{3}}{4}(\cos 2\alpha-1) & \frac{1}{2}\sin 2\alpha & 0 & 0 & \frac{3+\cos 2\alpha}{4} \end{bmatrix} \tag{2}$$

This expression contains the angular overlap model (AOM) parameters e_σ^N, $e_{\pi\|}^N$, e_ψ^N, e_x^N, and the bite angle δ. The dπ interactions in the plane of the bidentate are described by a single parameter $e_{\pi\|}^N$. In contrast the description of the out-of-plane dπ interactions requires two parameters, which are denoted as e_ψ^N and e_x^N. These parameters refer to $\pi_\perp$ interactions which are antisymmetrical and symmetrical, respectively, with respect to the $\mathscr{C}_2^\chi$ axis. The bidentate ligand must now be located in its actual coordination position. For a CuN_4Cl^+ complex of idealized C_{2v} symmetry this can be done by rotating the coordinate plane through an angle α about the x axis, starting from the reference position, as indicated in Fig. 4. The corresponding AOM rotation matrix, acting on the d-orbitals, is given by eqn. (2).

The angle α which denotes the bending of the plane containing the metal atom and the pair of nitrogen atoms with bite angle δ and azimuthal angle θ is given by:

$$\sin\alpha=\cos\theta/\cos\frac{\delta}{2} \tag{3}$$

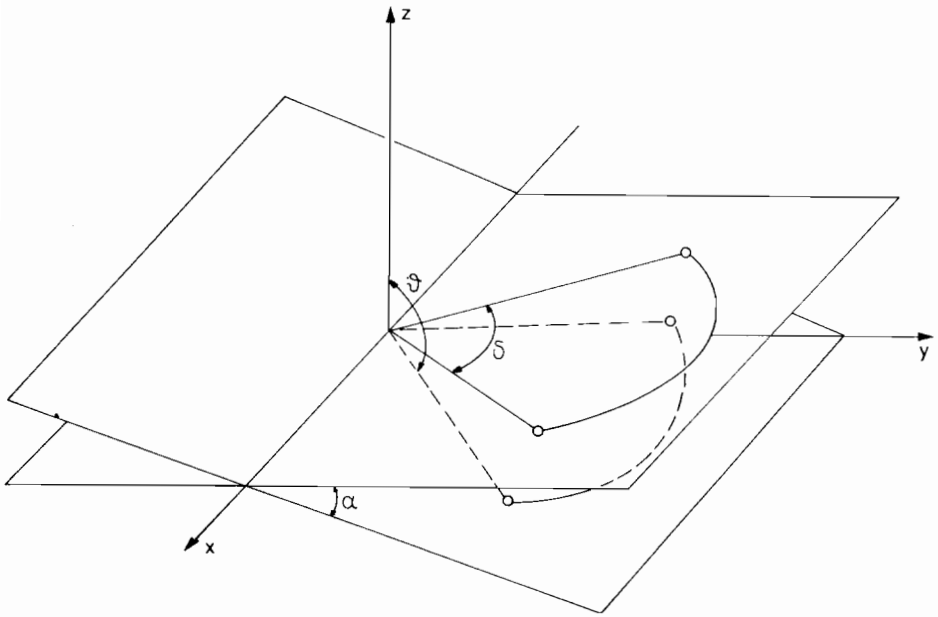

Fig. 4. Coordinate axes orientation and structural angles illustrating a bidentate ligand in the reference position (*xy* plane) and in a plane which is rotated over an angle α around the *x* axis. The angle δ is the bite angle, and θ is the azimuthal angle of the ligators (see also eqn. (3) in the text).

It should be noted that this rotation preserves coplanarity of the metal and the diimine bridge. This is in good agreement with the crystal structure, as can be seen from Fig. 1.

The full ligand field matrix for the CuN_4Cl^+ complex with idealized C_{2v} symmetry thus becomes:

$$\mathscr{H} = \mathscr{H}_{Cl} + \mathbb{F}(\mathscr{R}^x_\alpha)\mathscr{H}_{NN}\mathbb{F}(\mathscr{R}^x_\alpha)^{-1} + \mathbb{F}(\mathscr{R}^x_{-\alpha})\mathscr{H}_{NN}\mathbb{F}(\mathscr{R}^x_{-\alpha})^{-1} \quad (4)$$

Here $\mathscr{H}_{Cl}$ symbolizes the standard AOM matrix for a chloro-ligand on the positive *z* axis. The other two terms account for the diimine strands on the positive and negative *y* axis. For a qualitative discussion of the energy levels in the CuN_4Cl^+ complex it is instructive to place the four nitrogen ligators at the corners of a perfect square. In such a square pyramidal complex: $\cos\delta = \cos^2\theta$. Upon substitution, eqn. (4) yields:

$$\langle z^2|V|z^2\rangle = (3\cos^2\theta - 1)e_\sigma^N + e_\sigma^{Cl} - e_{ds} + \frac{3\sin^2 2\theta}{1+\cos^2\theta}[e_\psi^N + \cos^2\theta\, e_{\pi\parallel}^N]$$

$$\langle yz|V|yz\rangle = \frac{3}{2}\sin^2 2\theta\, e_\sigma^N + e_\pi^{Cl} + \frac{2(1-3\cos^2\theta)^2}{1+\cos^2\theta} e_\psi^N + \frac{8\cos^2\theta\sin^4\theta}{1+\cos^2\theta} e_{\pi\parallel}^N$$

$$\langle xz|V|xz\rangle = \frac{3}{2}\sin^2 2\theta\, e_\sigma^N + e_\pi^{Cl} + \frac{2\sin^4\theta}{1+\cos^2\theta} e_x^N + \frac{8\cos^6\theta}{1+\cos^2\theta} e_{\pi\parallel}^N$$

$$\langle xy|V|xy\rangle = 3\sin^4\theta\, e_\sigma^N + \frac{\sin^2 2\theta}{1+\cos^2\theta}[e_x^N + \cos^2\theta\, e_{\pi\parallel}^N]$$

$$\langle x^2-y^2|V|x^2-y^2\rangle = \frac{4\sin^2\theta}{1+\cos^2\theta}[\cos^2\theta\, e_\psi^N + e_{\pi\parallel}^N]$$

$$\langle z^2|V|x^2-y^2\rangle = \frac{\sqrt{3}\sin^2 2\theta}{1+\cos^2\theta}[e_\psi^N - e_{\pi\parallel}^N] \quad (5)$$

In this equation the energy of the d_{z^2} orbital has been lowered by an amount of $-e_{ds}$ to account for 3d–4s mixing [9, 10]. An estimate of this stabilizing interaction is given by the following simplified formula [9]:

$$e_{ds} = (3\cos^2\theta - 1)^2 e_\sigma^N + \tfrac{1}{4}e_\sigma^{Cl} + (3\cos^2\theta - 1)\sqrt{e_\sigma^N e_\sigma^{Cl}} \quad (6)$$

Using $e_\sigma^{Cl} = \frac{1}{2}e_\sigma^N$ and $\theta = 104°$, the energy lowering of the d_{z^2} orbital in the CuN_4Cl^+ square pyramid is calculated to be $-0.22e_\sigma^N$. This value is much smaller than the stabilization of one e_σ^N unit for a flat CuN_4^+ complex with no axial ligation [11]. It is clear that the presence of an apical ligand in combination with the non-planarity of the macrocyclic coordination gives rise to a much lower ds mixing effect, as compared to a strictly square planar complex where the effect is at its maximum. Equation (5) further illustrates the symmetry lowering role of the π bonding. In the case of isotropic π bonding, i.e. if $e_\psi^N = e_x^N = e_{\pi\parallel}^N$, the matrix elements in eqn. (5) will

reflect an effective D_{4h} symmetry, which is the holohedron symmetry of a regular square pyramid. This D_{4h} group contains two different orthorhombic subgroups. The subgroup with its three reflection planes in the Cartesian coordinate planes will be denoted as D_{2h}'. The other subgroup with vertical symmetry planes in between the x and y directions will be labeled D_{2h}''. Introduction of the anisotropic π bonding interactions of the diimine chelates will lower the tetragonal symmetry to D_{2h}'. In this symmetry group the matrix element between d_{z^2} and $d_{x^2-y^2}$ becomes symmetry allowed and the e_g level is split into xz and yz components. Both effects are indeed observed in eqn. (5). Especially the removal of the xz, yz degeneracy is of importance since it will affect the magnetic properties of the ground state. For $\theta = 104°$, eqn. (5) yields:

$$E(yz) - E(xz) = 1.3e_{\psi}^{N} - 1.7e_{\chi}^{N} + 0.4e_{\pi\|}^{N} \qquad (7)$$

For saturated bidentates this splitting is expected to be very small, since the e_{ψ}^{N} and e_{χ}^{N} parameters of such a chain are nearly identical. However this is not true if the bidentate bridge is a conjugated π chain, allowing direct electronic interactions between the $p\pi$ orbitals on the outer ligator atoms [12]. In such a case ψ- and χ-type interactions can even differ in sign [13–15]. As an example for the α-diimine strands in the $C_{10}H_{20}N_8$ macrocycle, the ligand LUMO is antisymmetric with respect to the C_2 axis of the chain, giving rise to a *π-acceptor* interaction of the ψ type, i.e. with $e_{\psi} < 0$. On the other hand the ligand HOMO is symmetric, so that the *π-donor* interaction is of the χ type, i.e. $e_{\chi} > 0$. Because of this sign difference both interactions cooperate to yield a large e_g splitting, with d_{xz} well above d_{yz}. This has indeed been confirmed by our recent EPR study of the analogous $Co(C_{10}H_{20}N_8)Cl_2$ compound, diluted in the Ni^{2+} salt [2]. It must be noted though that the e_g splitting decreases with increasing values of θ. Hence the CuN_4Cl^+ complex, which has the largest axial displacement of the metal, is expected to show the smallest e_g splitting.

A further aspect of the coordination geometry in the Cu^{2+} complex is the lengthening and bending of the N1–Cu–N10 bond axis, as compared to the N5–Cu–N14 axis. The corresponding perturbation has D_{2h}'' symmetry. Such a perturbation also lifts the degeneracy of the e_g level, now yielding $1/\sqrt{2}(d_{xz} + d_{yz})$ and $1/\sqrt{2}(d_{xz} - d_{yz})$ canonical components. Its primary effect though is the direct interaction between the d_{xy} and d_{z^2} orbitals which are both of a_g symmetry in D_{2h}''. According to the AOM the e_{σ} contribution to this interaction element is given by:

$$\langle d_{xy}|V|d_{z^2}\rangle = \sum_{L} \frac{\sqrt{3}}{4} (3\cos^2\theta_L - 1)\sin^2\theta_L \sin 2\varphi_L e_{\sigma}^{L} \qquad (8)$$

Here the summation involves the five ligator atoms of the CuN_4Cl^+ entity with θ_L and φ_L coordinates as specified in Table 4.

For a full treatment of the ligand field matrix one must of course resort to a computer program, which utilizes the actual coordination geometry. The algorithm for the introduction of anisotropic π bonding in bidentates at arbitrary angles has been described [13]. In the next section some results of ligand field calculations will be presented.

4.3. Ground state eigenvector

The d^9 configuration of the Cu^{2+} ion gives rise to five doublet states, which will be labeled with D_{4h} labels as $^2B_{2g}(xy)$, $^2B_{1g}(x^2-y^2)$, $^2E_g(xz)$, $^2E_g(yz)$, $^2A_{1g}(z^2)$. The principal component of the ground state eigenvector is the $^2B_{2g}$ state, with the unpaired electron in the highly antibonding d_{xy} orbital. The other states may mix in via spin–orbit coupling or low-symmetry components of the ligand field.

All our calculations have been based on the computer program STATE which diagonalizes the spin–orbit coupling and ligand field matrix for the d^9 configuration (see also ref. 16). It was found that perturbation theory could account very well for the form of the ground state eigenvector. This is of course related to the large energy separation between the $^2B_{2g}$ ground state and the interacting excited states. Accordingly in this section we will analyze the calculational results in the framework of perturbation theory.

If we limit ourselves to second order spin–orbit coupling and ligand field effects of D_{2h}' and D_{2h}'' symmetry, the following expressions for the Kramers components of the ground state can be obtained:

$$\begin{aligned} |E' + 1/2\rangle &= ia|^2B_{2g}xy\alpha\rangle + b|^2E_gxz\beta\rangle + c|^2B_{1g}x^2-y^2\alpha\rangle \\ &\quad - id|^2E_gyz\beta\rangle + ie|^2A_{1g}z^2\alpha\rangle \\ |E' - 1/2\rangle &= -ia|^2B_{2g}xy\beta\rangle - b|^2E_gxz\alpha\rangle + c|^2B_{1g}x^2-y^2\beta\rangle \\ &\quad - id|^2E_gyz\alpha\rangle - ie|^2A_{1g}z^2\beta\rangle \end{aligned} \qquad (9)$$

with $a^2 + b^2 + c^2 + d^2 + e^2 = 1$

In this equation $|^2B_{2g}xy\alpha\rangle$ denotes the d^9 determinantal function with the unpaired electron in the $d_{xy}\alpha$ spin–orbital etc... The form of the expansion has been chosen in such a way that the Kramers components obey the standard symmetry relationships [17] for real values of the eigenvector coefficients a, b, c, d, e. Approximate expressions for these coefficients can be derived from perturbation theory, and are given in eqn. (10).

$$a \approx 1$$

$$b \approx -\zeta/2[E(d_{xy}) - E(d_{xz})]$$

$$c \approx \zeta/[E(d_{xy}) - E(d_{x^2-y^2})]$$

$$d \approx -\zeta/2[E(d_{xy}) - E(d_{yz})]$$

$$e \approx \langle d_{xy}|V|d_{z^2}\rangle/[E(d_{xy}) - E(d_{z^2})] \quad (10)$$

The E values in this expression denote the one-electron orbital energies, that can be estimated from eqn. (5); ζ is the spin–orbit coupling constant for Cu^{2+}. In our calculations we have used a ζ value [18] of 700 cm^{-1}, compared with a value of 830 cm^{-1} in the free ion. In the complete calculations the a–e coefficients may acquire subsidiary imaginary components. As an example the mixing of d_{xz} and d_{yz} orbitals under a D_{2h}'' perturbation might give rise to imaginary components in the b and d coefficients. However in the present calculations such additional contributions were always verified to be at least one order of magnitude less important than the ones considered in eqn. (10). Several ligand field calculations have been performed, using representative parameter values and different symmetry constraints. The results are listed in Table 5.

The eigenvector coefficients in the Table can readily be understood on the basis of the perturbation expressions in eqn. (10). The D_{4h} starting point is characterized by $b = d$ and $e = 0$. This reflects respectively the initial degeneracy of the d_{xz} and d_{yz} levels, and the absence of a d_{z^2}–d_{xy} interaction element. In D_{2h}' the e_g degeneracy is lifted as a result of anisotropic π interactions (cf. eqn. (7)). Since the energy of d_{xz} is higher than the energy of d_{yz}, the $|^2E_g xz\rangle$ contribution to the ground state will become more prominent. On the other hand the effect of the D_{2h}'' perturbation is to introduce some d_{z^2} character in the ground state. The corresponding matrix element depends mainly on the bending of the N1–Cu–N10 axis, as compared to the N5–Cu–N14 axis (cf. eqn. (8)). The Table clearly shows that a combination of these tetragonal and orthorhombic perturbations is sufficient to explain the composition of the ground state in the final calculation with no symmetry constraints. In this calculation electronic transitions are computed at 14 960 ($xy \rightarrow z^2$) 16 420 ($xy \rightarrow xz$), 18 500 ($xy \rightarrow x^2$–y^2), and 18 920 ($xy \rightarrow yz$) cm^{-1}. We assign these transitions to a broad absorption band centered at about 16 800 cm^{-1} with an extinction coefficient of 220 l M^{-1} cm^{-1} which is observed in the visible spectrum of an aqueous solution of $Cu(C_{10}H_{20}N_8)Cl_2$.

TABLE 5. Ligand field calculations of the ground state eigenvector under different symmetry constraints

	D_{4h} [a]	D_{2h}' [b]	D_{2h}'' [c]	C_1 [d]
$a(xy)$	0.9989	0.9990	0.9978	0.9979
$b(xz)$	−0.0201	−0.0205	−0.0205	−0.0208
$c(x^2-y^2)$	0.0363	0.0356	0.0384	0.0374
$d(yz)$	−0.0201	−0.0178	−0.0213	−0.0185
$e(z^2)$			0.0441	0.0434

[a]Square pyramidal geometry with $\theta = 104°$; AOM parameters (in cm^{-1}): $e_\sigma^{Cl} = 3000, e_{ds} = 2150, e_\pi^{Cl} = 500, e_\sigma^N = 8000, e_{\pi\parallel}^N = e_\psi^N = e_\chi^N = 700$, $\zeta = 700$. [b]Same as D_{4h}, but with: $e_\psi^N = -1000$, $e_\chi^N = +1000$ (cf. ref. 15). [c]Experimental geometry (cf. Table 4); AOM parameters as in D_{4h}, but with $e_\sigma^{N1} = e_\sigma^{N10} = 7700$, $e_\sigma^{N5} = e_\sigma^{N14} = 8000$. [d]Experimental geometry; e_σ^N parameters as in [c], e_π^N parameters as in [b].

4.4. g Tensor

In this section we discuss the EPR spectra from the point of view of the extended AOM model, presented in the previous sections. Because of the many parameters involved, a detailed fit of the g tensor to AOM expressions is to some extent arbitrary. Hence our treatment will be limited to a few sample calculations, which clearly illustrate the orthorhombic features of the spectrum.

The g tensor for the ground state of the $Cu(C_{10}H_{20}N_8)Cl_2$ complex can be expressed as a function of the coefficients in eqn. (9). One obtains:

$$g_{xx} = 2.0023(-a^2 - b^2 + c^2 + d^2 - e^2) + 4ab + 4cd$$

$$g_{yy} = 2.0023(-a^2 + b^2 + c^2 - d^2 - e^2) + 4ad + 4bc$$

$$g_{xy} = 4\sqrt{3}de$$

$$g_{yx} = 4\sqrt{3}be$$

$$g_{zz} = 2.0023(a^2 - b^2 + c^2 - d^2 + e^2) + 8ac - 4bd$$

$$g_{xz} = g_{zx} = g_{yz} = g_{zy} = 0$$

If the off-diagonal elements, g_{xy} and g_{yx}, are non-zero, the principal in-plane g values, g_2 and g_3, can be obtained by diagonalizing the $(g)^2$ tensor [19]. These components are rotated with respect to the Cartesian x and y axes over an angle θ_g, which is defined as follows:

$$\tan(2\theta_g) = \frac{2(g_{xx}g_{yx} + g_{yy}g_{xy})}{g_{xx}^2 + g_{xy}^2 - g_{yy}^2 - g_{yx}^2} \quad (12)$$

In Table 6 we present the calculated g values for the different symmetry cases considered. In these calculations the orbital contributions to the g elements were attenuated by an isotropic reduction factor [18] of 0.75.

TABLE 6. Calculated g tensor under different symmetry constraints[a]

	D_{4h}	D_{2h}'	D_{2h}''	C_1	Observed
g_{zz}	2.218	2.214	2.229	2.225	2.178
g_{xx}	−2.058	−2.059	−2.058	−2.059	
g_{yy}	−2.058	−2.051	−2.061	−2.052	
g_{xy}	0	0	−0.005	−0.004	
g_{yx}	0	0	−0.005	−0.005	
$\lvert g_2\rvert$ [b]	$g_\perp$	g_{xx}	2.065(53°)	2.061(26°)	2.066(45°)
$\lvert g_3\rvert$ [b]	$g_\perp$	g_{yy}	2.054(−37°)	2.050(−64°)	2.048(−45°)

[a]Calculated from eqn. (10) using the eigenvector coefficients of Table 5. Orbital contributions were attenuated by an isotropic reduction factor of 0.75. [b]The values in brackets are angles with respect to the x axis. The N1–Cu–N10 direction is at 48°.

For the D_{4h} case one has an axial g tensor with $g_{\parallel}=2.218$, $g_{\perp}=2.058$. These values are close to the observed g values of the powder spectrum ($g_{\parallel}=2.183$, $g_{\perp}=2.047$). They are also in line with the EPR spectra of several related macrocyclic Cu^{2+} complexes [4, 20–23]. The $(g_{\parallel}-2)/(g_{\perp}-2)$ ratio is nearly equal to 4, which is characteristic for the Cu^{2+} ion in a square-based pyramidal or bipyramidal coordination [18]. In the orthorhombic cases, D_{2h}' and D_{2h}'', the g tensor is anisotropic in the xy plane, principal g values being directed along the respective twofold axes. In D_{2h}' the largest in-plane g value is found in the x direction, i.e. perpendicular to the bisector of the α-diimine bridges. As we have explained, this anisotropy is due to the π-bonding of the unsaturated macrocyclic strands. It should be noted that the calculated effect is very small ($\Delta g \approx 0.01$). Far larger anisotropies ($\Delta g \approx 2$) can be observed in analogous Co^{2+} complexes [2, 17, 24]. On the other hand if the symmetry of the ligand field is D_{2h}'', the g values are rotated over $\pi/4$ to coincide with the metal–ligand bond axes. According to Hitchman's rule the larger g value should be along the weaker axis [25, 26]. In the column marked D_{2h}'' of Tables 5 and 6 we have investigated the ligand field at the experimental geometry, assuming isotropic π-bonding. The results have approximate D_{2h}'' symmetry, i.e. $g_{xx} \approx g_{yy}$ and $g_{xy} \approx g_{yx} \neq 0$. The larger g value is found near the N1–Cu–N10 axis, which is more bent and slightly more elongated than the N5–Cu–N14 axis. This result thus confirms Hitchman's rule. Apparently the mixing of d_{xz} and d_{yz} orbitals under a D_{2h}'' perturbation has no sizeable effect on the $g_{\perp}$ anisotropy, as compared to the effect of d_{xy}–d_{z^2} mixing. This is often the case if there is a significant orthorhombic distortion [27].

Finally in the C_1 ligand field calculation the principal g values are found to be in between the D_{2h}' and D_{2h}'' results. This is of course a direct consequence of the comparable magnitude of both perturbations, each giving rise to a Δg anisotropy of about 0.01. In contrast in the observed EPR spectra the g tensor is very close to the D_{2h}'' results, with $\Delta g \approx 0.02$. This implies that the D_{2h}'' perturbation is the dominant one, at least as far as the g tensor is concerned. The observed g_2 is along the N1–Cu–N10 axis, which is in line with the predictions of the D_{2h}'' scheme.

4.5. A Tensors

Simplified theoretical expressions [28] for the Cu^{2+} hyperfine tensor in axial symmetry are given by:

$$A_{\parallel} = P\left[-\left(\frac{4}{7}+\kappa\right)+(g_{\parallel}-2.0023)+\frac{3}{7}(g_{\perp}-2.0023)\right]$$

$$A_{\perp} = P\left[\frac{2}{7}-\kappa+\frac{11}{14}(g_{\perp}-2.0023)\right] \qquad (13)$$

where κ is the Fermi contact parameter. Axial A values may be calculated from Table 3, yielding: $|A_{\parallel}|=178\ 10^{-4}\ cm^{-1}$, $|A_{\perp}|=35\ 10^{-4}\ cm^{-1}$. With $A_{\parallel}<0$, eqn. (13) is satisfied by taking $P=320\ 10^{-4}\ cm^{-1}$, $\kappa=0.22$ or $P=220\ 10^{-4}\ cm^{-1}$, $\kappa=0.49$ according to the choice of sign for $A_{\perp}$. These parameter ranges are in agreement with published values [20, 22, 29]. For a discussion of the non-axial features of the hyperfine spectrum, the elements of the A tensor must be expressed as functions of the eigenvector coefficients. The results of such calculations are very similar to the g tensor results of the preceding section. As an example under a dominant D_{2h}'' perturbation, which is apparently required to explain the experimental g tensor, the principal in-plane components, A_2 and A_3, are predicted to be directed along the bond axes. This is of course in marked contrast with the experimental orientation of the A tensor, which almost coincides with the bisector directions (cf. Fig. 3). However even a D_{2h}' calculation yields unsatisfactory results since the calculated in-plane anisotropy is almost one order of magnitude too small.

Hence we must conclude that a parametric ligand-field model is unable to explain the anisotropy of the Cu hyperfine tensor. In this respect it is noteworthy that spin-unrestricted Xα-SW calculations of Maroney *et al.* [30] on a bis-α-diimine $Cu(N_2C_2H_4)_2^{2+}$ model with D_{2h}' symmetry yielded: $A_{xx}=-65\ 10^{-4}\ cm^{-1}$, $A_{yy}=-42\ 10^{-4}\ cm^{-1}$. Although the magnitude of this ΔA anisotropy is of the right order, the relative ordering of A_{xx} and A_{yy} still contrasts with our experimental findings.

Finally we note that the superhyperfine tensor for the nitrogen ligators is almost isotropic. This is in line with previously observed trends [4, 20, 23]. In most of these studies in plane variations of the A^N tensor remained undetected, because of the small anisotropy of the g tensor itself.

5. Discussion

An interesting feature of the EPR spectrum of the $Cu(C_{10}H_{20}N_8)Cl^+$ complex is the non-coincidence of the principal axes of the g and A^{Cu} tensors. In slightly anisotropic media such orientational differences are not uncommon, due to the near axial degeneracy of both tensors [31]. As an example Keijzers and coworkers have reported non-coincidence of the principal axes in several diseleno and dithiocarbamate complexes of divalent copper [32, 33]. What is rather remarkable in the present complex is that both the g and A^{Cu} tensors are oriented along special molecular axes. The g tensor is almost collinear with the frame of the bond axes, while the A tensor is clearly oriented along the bidentate

bisectors. From a symmetry point of view these two frames can be related to the two orthorhombic subgroups of the tetragonal D_{4h} group. As we have shown, the ligand field of the $C_{10}H_{20}N_8$ macrocycle indeed contains both types of D_{2h} perturbations. The orientation of the g tensor could thus be shown to be due to differences in the two N–Cu–N bond axes. Similar effects are also observable in saturated macrocyclic complexes [26]. In contrast the orientation of the A tensor is seen to follow the anisotropy of the π-bonding interactions of the unsaturated parts in the tetraimine chain. This effect seems to be much more pronounced than would be expected on the basis of AOM type calculations, and is probably due to differences in covalency along the x and y directions.

Acknowledgements

The authors thank Professor M. A. Hitchman for valuable suggestions relating to this work. The research at the laboratory of quantum chemistry was supported by a grant of the Belgian Government (Programmatie van het Wetenschapsbeleid). A.C. is indebted to the Belgian National Science Foundation (NFWO) for financial support. F.D. acknowledges support from the Fonds National Belge de la Recherche Scientifique (FNRS). Thanks are also due to Professor P. Piret for Weissenberg measurements.

References

1 S.-M. Peng, G. C. Gordon and V. L. Goedken, *Inorg. Chem., 17* (1978) 119.
2 A. Ceulemans, R. Debuyst, F. Dejehet, G. S. D. King, M. Vanhecke and L. G. Vanquickenborne, *J. Phys. Chem., 94* (1990) 105.
3 S. R. Hall and J. M. Stewart (eds.), *XTAL 2.6 User's Manual*, Universities of Western Australia and Maryland, 1989.
4 M. J. Maroney and N. J. Rose, *Inorg. Chem., 23* (1984) 2252.
5 O. P. Anderson and J. C. Marshall, *Inorg. Chem., 17* (1978) 1258.
6 O. P. Anderson and A. B. Packard, *Inorg. Chem., 18* (1979) 1940; *18* (1979) 3064; *19* (1980) 2123; *19* (1980) 2941.
7 E. Schifflers and R. Debuyst, *J. Magn. Reson., 14* (1974) 85.
8 A. Ceulemans and L. G. Vanquickenborne, *Pure Appl. Chem., 62* (1990) 1081.
9 A. Ceulemans, D. Beyens and L. G. Vanquickenborne, *Inorg. Chim. Acta, 61* (1982) 199.
10 D. W. Smith, *Inorg. Chim. Acta, 22* (1977) 107.
11 M. A. Hitchman and J. B. Bremner, *Inorg. Chim. Acta, 27* (1978) L61.
12 L. E. Orgel, *J. Chem. Soc.,* (1961) 3683.
13 A. Ceulemans, M. Dendooven and L. G. Vanquickenborne, *Inorg. Chem., 24* (1985) 1153.
14 H. Yamatera and C. E. Schäffer, presented at the *XXIV Int. Conf. Coord. Chem., Athens, Aug., 1986,* Abstract.
15 M. Atanasov and T. Schönherr, *Inorg. Chem., 29* (1990) 4545.
16 A. Bencini, C. Benelli and D. Gatteschi, *Coord. Chem. Rev., 60* (1984) 131.
17 A. Ceulemans, M. Dendooven and L. G. Vanquickenborne, *Inorg. Chem., 24* (1985) 1159.
18 B. J. Hathaway and D. E. Billing, *Coord. Chem. Rev., 5* (1970) 143.
19 J. E. Wertz and J. R. Bolton, *Electron Spin Resonance,* McGraw-Hill, New York, 1972, p. 137.
20 V. Malatesta and B. R. McGarvey, *Can. J. Chem., 53* (1975) 3791.
21 Y. Nishida, K. Hayashida, A. Sumita and S. Kida, *Inorg. Chim. Acta, 31* (1978) 19.
22 Y. Nishida, K. Hayashida and S. Kida, *J. Coord. Chem., 10* (1980) 101.
23 M. Pasenkiewicz-Gierula, W. E. Antholine, W. K. Subczynski, O. Baffa, J. E. Hyde and D. H. Petering, *Inorg. Chem., 26* (1987) 3945.
24 C. Daul, C. W. Schläpfer and A. von Zelewsky, *Struct. Bonding (Berlin), 36* (1979) 129.
25 M. A. Hitchman, *J. Chem. Soc. A,* (1970) 4.
26 M. A. Hitchman, L. Kwan, L. N. Engelhardt and A. H. White, *J. Chem. Soc., Dalton Trans.,* (1987) 457.
27 M. A. Hitchman, C. D. Olson and R. L. Belford, *J. Chem. Phys., 50* (1969) 1195.
28 A. Abragam and B. Bleaney, *Electron Paramagnetic Resonance of Transition Ions,* Clarendon, Oxford, 1970, p. 456.
29 R. Debuyst, F. Dejehet, C. Görller-Walrand and L. G. Vanquickenborne, *Inorg. Chim. Acta, 36* (1979) 275.
30 M. J. Maroney, J. G. Norman and J. H. Osborne, *Inorg. Chem., 23* (1984) 2261.
31 E. Buluggiu and A. Vera, *J. Chem. Phys., 59* (1973) 2886.
32 J. G. M. Van Rens, C. P. Keijzers and H. Van Willigen, *J. Chem. Phys., 52* (1970) 2858.
33 C. P. Keijzers and E. de Boer, *Mol. Phys., 29* (1975) 1743.